J. Phys.: Condens. Matter **24** (2012) 036001 (5pp) doi:10.1088/0953-8984/24/3/036001

Incommensurate magnetic order in $TbTe_3$

F Pfuner[1], S N Gvasaliya[1,2], O Zaharko[2], L Keller[2], J Mesot[1,2], V Pomjakushin[2], J-H Chu[3,4], I R Fisher[3,4] and L Degiorgi[1]

[1] Laboratory for Solid State Physics, ETH Zürich, CH-8093 Zürich, Switzerland
[2] Laboratory for Neutron Scattering, PSI, CH-5232 Villigen, Switzerland
[3] Geballe Laboratory for Advanced Materials and Department of Applied Physics, Stanford University, Stanford, CA 94305, USA
[4] Stanford Institute of Energy and Materials Science, SLAC National Accelerator Laboratory, 2575 Sand Hill Road, Menlo Park 94025, CA 94305, USA

E-mail: sgvasali@phys.ethz.ch

Received 6 October 2011, in final form 10 November 2011
Published 9 December 2011
Online at stacks.iop.org/JPhysCM/24/036001

Abstract
We report a neutron diffraction study of the magnetic phase transitions in the charge-density wave (CDW) $TbTe_3$ compound. We discover that in the paramagnetic phase there are strong 2D-like magnetic correlations, consistent with the pronounced anisotropy of the chemical structure. A long-range incommensurate magnetic order emerges in $TbTe_3$ at $T_{mag1} = 5.78$ K as a result of continuous phase transitions. We observe that near the temperature T_{mag1} the magnetic Bragg peaks appear around the position (0, 0, 0.24) (or its rational multiples), that is fairly close to the propagation vector (0, 0, 0.29) associated with the CDW phase transition in $TbTe_3$. This suggests that correlations leading to the long-range magnetic order in $TbTe_3$ are linked to the modulations that occur in the CDW state.

(Some figures may appear in colour only in the online journal)

1. Introduction

The RTe_3 family of compounds (R = rare earth) have recently attracted renewed interest as a model system for layered (two-dimensional) charge-density wave (CDW) materials. RTe_3 crystallizes in an orthorhombic structure, composed of double layers of planar Te sheets separated by corrugated R–Te layers. The average chemical structure can be described using the *Cmcm* space group [1] (in this setting the lattice parameters a and c are close to each other, whereas b is approximately six times longer), although in these materials an incommensurate lattice modulation with a wavevector $q_c \sim 2/7c^*$ is observed below the phase transition into the CDW state [2, 3]. Such a CDW state with modulations along the c-axis is present in all RTe_3 materials. However, the members with the heaviest rare-earth elements exhibit a second CDW phase transition at lower temperatures that is characterized by a modulation wavevector $q_a \sim 1/3a^*$ [4, 5]. The temperatures of these two CDW transitions show opposite trends as a function of the R-atom mass. Whereas T_{CDW1} decreases toward heavier members of the family (i.e., going from La to Tm), the T_{CDW2} associated with the a-axis incommensurability is higher for heavier compounds [4, 6]. For the specific compound studied in this report, $TbTe_3$, transport and diffraction experiments yield $T_{CDW1} = 336$ K. Although transport measurements do not clearly reveal the presence of a second CDW transition, STM measurements performed at 6 K do show an ordering pattern that is associated with the wavevector $\sim 2/3a^*$ [5]. More recent high resolution x-ray diffraction measurements confirm the presence of a transverse CDW at low temperatures, with wavevector $\sim 0.683a^*$, although T_{CDW2} is at present unknown [7].

The RTe_3 family appears to be a classic CDW system, for which the CDW wavevector corresponds to an enhancement of the generalized susceptibility $\chi(q)$, which is largely driven by Fermi surface nesting [8–10]. The enhancement is, however, far from being a divergence, suggesting an important role for strong electron–phonon coupling [10]. The Fermi surface is composed of states associated with the double Te layers, and is therefore similar for all members of the series. The principal role of the rare-earth ion R appears to be chemical pressure, which only modestly affects the resulting CDW wavevectors [2, 4].

In addition to hosting an incommensurate CDW, for magnetic rare-earth ions, RTe_3 also hosts long-range antiferromagnetic order at low temperatures. The magnetic phase transitions of RTe_3 have been studied using magnetization [6, 11–13], calorimetry [6, 11, 13] and electrical resistivity [6, 11–13]. Using these macroscopic techniques the temperatures of the magnetic transitions have been determined and a phase diagram summarizing the temperatures of CDW and magnetic phase transition of RTe_3 has been established in [6]. However, the nature of the long-range magnetic order in this family of compounds has not yet been studied by diffraction techniques, and the effect of the incommensurate lattice modulation on the magnetic structure is unknown. To bridge this gap we have performed neutron scattering experiments in the representative compound $TbTe_3$. The choice of this material was dictated by the following reasons. In order to establish a possible relationship of the propagation vectors associated to the CDW state and of the long-range magnetic order one needs to study a material that has reasonably close values between T_{CDW2} and T_N. Based on this condition, $DyTe_3$ and $TbTe_3$ are both attractive candidates according to their phase diagram [6]. $DyTe_3$ undergoes two magnetic phase transitions at $T \sim 3.6$ and ~3.45 K [6]. However, due to the high absorption of Dy the neutron measurements on $DyTe_3$ are too challenging[5]. $TbTe_3$ exhibits three closely located magnetic phase transitions at the following temperatures: $T_{mag1} = 5.78$ K, $T_{mag2} = 5.56$ K and $T_{mag3} = 5.38$ K [6]. Here, we present a study of the magnetic phase transitions in $TbTe_3$ using powder and single-crystal neutron diffraction.

2. Experimental techniques

Single crystals of $TbTe_3$ were grown by slow cooling a binary melt, as described elsewhere [11]. As the material is rather air-sensitive, the $TbTe_3$ powder was obtained by crushing the single crystals in He atmosphere. The powder was immediately sealed in a cylindrical vanadium can of 6 mm in diameter used for the measurements.

Powder neutron diffraction experiments were performed at the DMC cold neutron diffractometer [14] (neutron spallation source SINQ [15], PSI) in the temperature range 1.5–60 K. Most of the data were collected with neutron wavelengths of $\lambda = 2.46$ Å, giving access to the wavevector range 0.1–3.4 $Å^{-1}$. Typical exposure times were ~12 h.

The experiments on the single crystals of $TbTe_3$ with size of roughly $\sim 7 \times 8 \times 2.5$ mm^3 were performed at the TriCS single-crystal diffractometer [16]. A pyrolytic graphite (PG) monochromator was used with neutron wavelength $\lambda = 2.32$ Å. A 120 mm long PG filter was installed in the beam in order to ensure full suppression of higher-order neutrons. The temperature range of interest for these measurements is $T \sim 2$–8 K, because the three magnetic phase transitions are close to each other in the range 5–6 K. This interval was scanned with steps of ~0.05 K. To ensure the required accuracy in temperature an 'orange'-type He flow cryostat was used. One of the samples was aligned in the $[H, K, 0]$ plane and a second sample was aligned in the $[0, K, L]$ plane. The normal beam geometry was employed, tilting the detector in the range of $-10°$–$10°$. This allowed us to access reflections with $L = \pm 1$ and $H = \pm 1$, respectively.

[5] In fact we made a trial and performed a neutron powder diffraction experiment on $DyTe_3$ packed into a double wall vanadium container. However, with the exception of the two most intense peaks, the signal to noise ratio was not favorable for reliable conclusions. Therefore, we do not report the neutron scattering results obtained for $DyTe_3$ and concentrate here on $TbTe_3$.

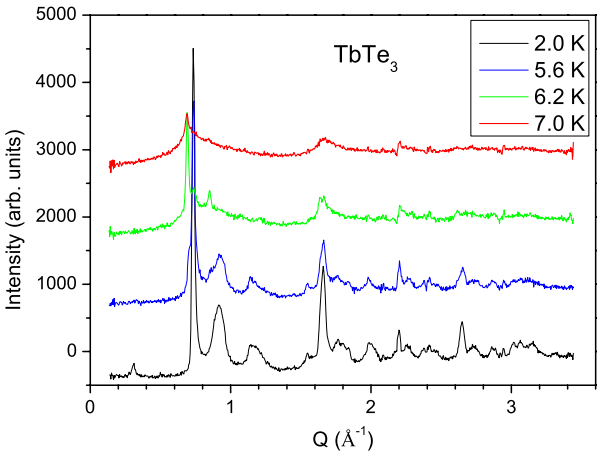

Figure 1. Temperature dependence of the difference patterns with respect to the data at the reference temperature of 60 K. For clarity, the patterns obtained at increasing temperatures are progressively shifted in vertical scale by 1000. The pronounced negative values in the difference patterns at $|Q| < 1.5$ $Å^{-1}$ are due to the strong wavevector-dependent paramagnetic scattering observed in $TbTe_3$ at $T = 60$ K.

3. Powder diffraction results

The data at 60 K were taken as a reference for the scattering in the paramagnetic phase of $TbTe_3$. We did not observe any superlattice peak that could correspond to the lattice modulation caused by the CDW order in $TbTe_3$. The average chemical structure of $TbTe_3$ was refined with Fullprof [17] within the *Cmcm* space group following a structural model of the RTe_3-type materials developed in [18]. This analysis indicates the presence of several preferred orientations in the sample, impeding high-quality refinements of both chemical and magnetic structures. Nevertheless, the lattice parameters obtained from the data, $a = 4.3050 \pm 0.000\,15$ Å, $b = 25.337\,57 \pm 0.0012$ Å, and $c = 4.280\,24 \pm 0.000\,12$ Å, are in agreement with those published earlier [18]. In what follows we concentrate on the differences of the data taken at temperatures lower than 60 K. In this experimental setup the low-temperature changes in the chemical structure of $TbTe_3$ are not resolved.

Figure 1 shows difference patterns at selected temperatures, obtained by eliminating the contribution from the chemical structure by the subtraction of the diffraction pattern at 60 K. As expected from the macroscopic properties of $TbTe_3$, magnetic Bragg peaks appear in the diffraction patterns collected below $T_{mag1} = 5.78$ K. Furthermore,

relatively sharp asymmetric peaks appear in the diffraction patterns even at temperatures slightly higher than T_{mag1} (e.g., the patterns taken at 6.2 K and 7 K). As shown in figure 1, these unusual peaks have an extended shoulder toward higher wavevectors. Such scattering profiles from powders are typical for systems with pronounced quasi-two-dimensional (quasi-2D) properties, as observed, e.g., in graphite [19] or in 2D magnetic materials [20]. Therefore, one may expect that in a relatively broad temperature range above T_{mag1} $TbTe_3$ exhibits quasi-2D behavior. The positions of the magnetic Bragg peaks are temperature-dependent and may be clearly distinct in different magnetic phases. This suggests that the magnetic phases occurring in $TbTe_3$ are modulated and the propagation vector is locked-in at an incommensurate position only below T_{mag3}. In addition, the asymmetric peaks above T_{mag1} are located at a different wavevector as compared to the magnetic Bragg peaks observed just below T_{mag1}. This is best seen in the scattering profiles shown in figure 1 in the vicinity of $\mathbf{Q} \sim 0.7$ Å^{-1}.

Figure 2 shows the magnetic diffraction pattern measured in $TbTe_3$ at 2 K. Some of the magnetic peaks could be indexed in terms of the average chemical cell and are labeled in figure 2 (due to the complexity of the pattern the use of single-crystal neutron diffraction data was essential for this step). Clearly, most of the magnetic Bragg peaks are at positions incommensurate with the average chemical structure of the material. It may be speculated that the broad magnetic peaks observed in the vicinity of $Q \simeq 0.9$ and $\simeq$1.2 Å are composed of many magnetic Bragg peaks which are located close to each other in wavevector space, due to the rather large value of the lattice parameter b. We note here that among the magnetic Bragg peaks we could not identify any with non-zero value of H.

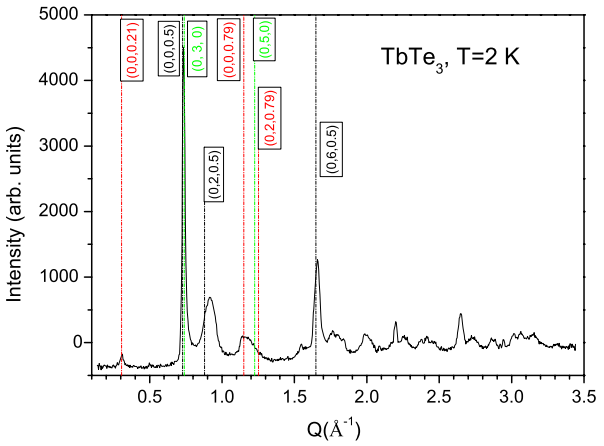

Figure 2. Indexed magnetic reflections for $TbTe_3$ at 2 K in a powder diffraction pattern (the contribution from the chemical structure is eliminated by subtracting the powder spectrum taken at $T = 60$ K). The indexed peaks were identified by single-crystal neutron diffraction experiments. The labels in the brackets are the (H, K, L) indices of the peaks given in terms of the average *Cmcm* structure. The peaks that are associated with the magnetic propagation vector $q_1^{\mathrm{mag}} = (0, 0, 0.21)$ are labeled in red, those associated with the magnetic propagation vector $q_2^{\mathrm{mag}} = (0, 0, 0.5)$ are shown in black, and, finally, those associated with $q_3^{\mathrm{mag}} = (0, 1, 0)$ are shown in green. Note that the Bragg peaks that are labeled for simplicity as $(0, K, L) \pm (0, 0, 0.21)$ in fact have a non-zero component of modulation along the $(\langle 0, K, 0\rangle)$ direction and more precisely should be described as $(0, K, L) \pm (0, 0.01, 0.21)$. See text and figure 4 for details.

4. Single-crystal diffraction results

Taking into account the complexity of the powder diffraction patterns observed in the magnetically ordered phases of $TbTe_3$, there are considerable difficulties not only in developing a proper model of the arrangement of the Tb magnetic moments, but even in determining the propagation vectors in the magnetically ordered phases. In a trial to overcome these difficulties a series of single-crystal experiments were performed at the base temperature $T = 2$ K, below T_{mag3}. Those reflections which were successfully indexed at $T = 2$ K are labeled in figure 2. There was no attempt to index the peaks observed in the powder diffraction patterns at higher temperatures. Instead, the temperature evolution of those peaks that were identified at $T = 2$ K was traced up to $T \sim 7$ K.

Figure 3 shows false-color maps of neutron intensities taken in close vicinity to the $(0, 0, 0.21)$ incommensurate magnetic reflection in the temperature range 1.5–6 K. At the base temperature this reflection has incommensurate components along both the $\langle 0, K, 0\rangle$ and $\langle 0, 0, L\rangle$ directions. However, the incommensurate component along the $\langle 0, K, 0\rangle$ direction appears to be small and diminishes above T_{mag3} in a step-like way. Above T_{mag3} the incommensurate component along the $\langle 0, 0, L\rangle$ direction is also temperature-dependent. For a more quantitative analysis the scans for each temperature are fitted assuming a Gaussian shape for a Bragg reflection. The resulting temperature dependences of the position and intensity of the peak $(0, 0, 0.21)$ are shown in figure 4. The modulation vector along the $\langle 0, 0, L\rangle$ direction stays constant within the precision of the measurements below T_{mag3}. Above T_{mag3} the propagation vector increases smoothly and reaches the value of $(0, 0, 0.242 \pm 0.001)$ at T_{mag1}. The modulation vector along the $\langle 0, K, 0\rangle$ direction is also constant at $(0, 0.01 \pm 0.001, 0)$ below T_{mag3}, while above this temperature the component of the modulation vanishes. The intensity measured around the $(0, 0, 0.21)$ position also appears to be nearly temperature-independent below T_{mag3}. Above this temperature, however, the overall intensity observed in the vicinity of the $(0, 0, 0.21)$ position drops by a factor of 2, as can be deduced from figures 4(b)–(d). Further the intensity gradually decreases and above T_{mag1} we could not detect any scattering above the background level around that position. In the whole studied temperature range the width of the peaks is limited by the resolution. The gradual decrease of the Bragg intensity suggests a continuous character of the phase transition that the crystal undergoes at T_{mag1}, whereas an abrupt change in magnetic intensity at T_{mag3} points to a first order phase transition.

The magnetic Bragg peaks, characterized by the propagation vector $(0, 0, 0.5)$, exhibit a qualitatively different behavior. Figure 5 shows the temperature dependence of the $(0, 4, 0.5)$ Bragg peak in the temperature range 4–6 K as a

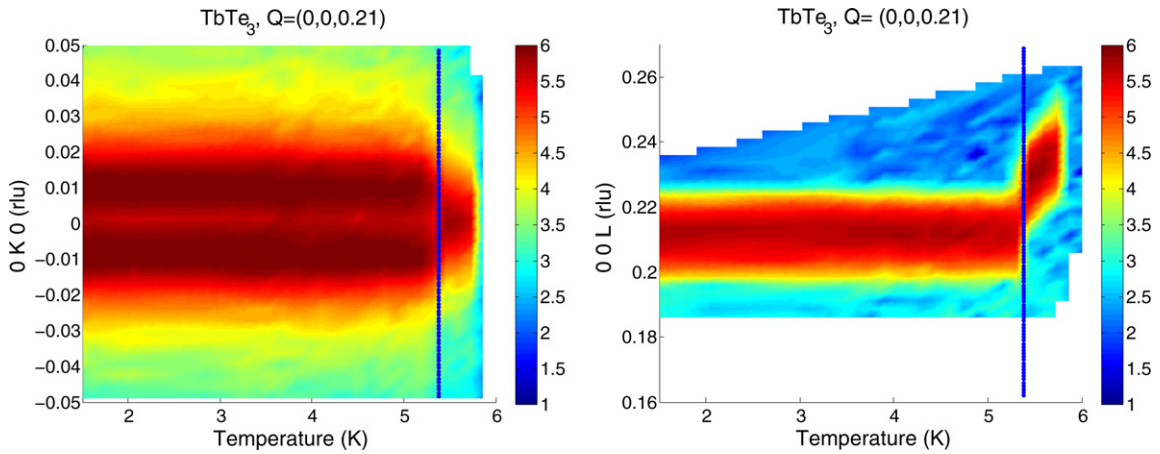

Figure 3. The temperature evolution of the intensity distribution taken in the vicinity of the (0, 0, 0.21) position of $TbTe_3$. The vertical solid lines in both plots denote $T_{mag3} = 5.38$ K. Note that below T_{mag3} the reflection is incommensurate in both the $\langle 0, K, 0\rangle$ and $\langle 0, 0, L\rangle$ directions.

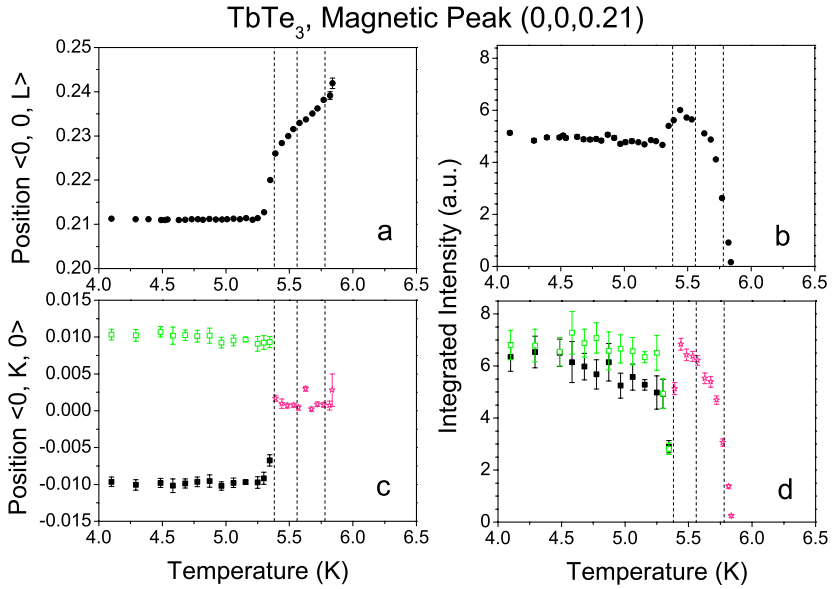

Figure 4. The temperature evolution of the propagation vectors (left column) and of the intensity (right column) measured around the position (0, 0, 21). The green symbols denote the position and the intensity of the $(0, 0 + \delta, 0.21)$ satellite, whereas the black squares stand for the $(0, 0 - \delta, 0.21)$ satellite. The vertical dashed lines denote the temperatures of the magnetic phase transitions.

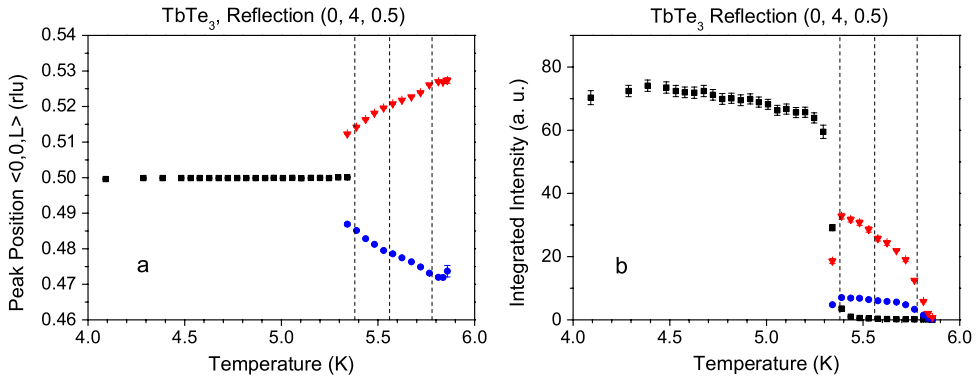

Figure 5. The temperature evolution of the intensity distribution taken in the vicinity of the (0, 4, 0.5) position of $TbTe_3$. The red triangles show the position and the intensity of the $(0, 0, 0.5 + \delta)$ satellite, while the blue circles denote the position and the intensity of the $(0, 0, 0.5 - \delta)$ satellite. The vertical dashed lines denote the temperatures of the magnetic phase transitions.

representative example. Whereas below T_{mag3} the propagation vector is (0, 0, 0.5), above this temperature the position of the magnetic Bragg peaks becomes incommensurate in a step-like fashion as (0, 0, 0.5 ± δ), with δ displaying a temperature dependence. The intensity of the (0, 4, 0.5) magnetic peak decreases abruptly at T_{mag3} and smoothly diminishes toward T_{mag1}. Weak magnetic peaks around the (0, 4, 0.5) position are still observed in the paramagnetic phase up to ∼6 K.

5. Discussion and conclusions

We have performed a first study of the magnetic phase transitions in $TbTe_3$ by powder and single-crystal neutron diffraction. We find that in the paramagnetic phase, slightly above $T_{mag1} = 5.78$ K, there are pronounced 2D-like magnetic correlations. At T_{mag1} long-range magnetic order emerges as a result of a continuous phase transition. In all three magnetically ordered phases, incommensurate modulations are present. This observation is at variance with the typical behavior of unmodulated rare-earth intermetallic compounds (see e.g. [21, 22]). Incommensurate magnetic structures often appear in these materials just below the phase transition into the magnetically ordered state. However, in most cases magnetoelastic coupling and crystal-field effects typically result in a lock-in transition to a commensurate magnetic structure. The behavior found in $TbTe_3$ only partially resembles these general expectations. As shown in figure 5, the magnetic propagation vector of the (0, 0, 0.5±δ)-type observed just below T_{mag1} turns out to be locked-in below T_{mag3} in the simple antiferromagnetic position (0, 0, 0.5). However, the magnetic Bragg peaks observed below T_{mag1} near the position (0, 0, 0.24) stabilize at low temperature at the incommensurate position (0, 0 + δ, 0.21). This effect is possibly due to the incommensurate lattice modulation present in $TbTe_3$ in the CDW state.

The propagation vectors of the magnetic structures, which we succeeded in identifying in $TbTe_3$, have components along either the $\langle 0, K, 0\rangle$ or $\langle 0, 0, L\rangle$ directions, or a linear combination of both. We could not assign any of the magnetic peaks observed in the powder diffraction pattern as a Bragg reflection with non-zero component $\langle H, 0, 0\rangle$ of the propagation vector. Therefore, our results do not point toward a link of the propagation vector associated with the second CDW phase transition and the magnetic order in $TbTe_3$. Nonetheless, we discover that near the temperature T_{mag1} the magnetic Bragg peaks appear around the positions (0, 0, 0.24) (or its rational multiples). This value is fairly close to the propagation vector (0, 0, 0.29) [4] associated with the high-temperature CDW phase transition, raising the possibility that the correlations leading to the long-range magnetic order in $TbTe_3$ might be linked to the modulated chemical structure in the CDW state. These results should stimulate further work to refine the magnetic structure in this and related magnetic RTe_3 compounds, with the ultimate goal of establishing how the CDW and magnetic order interact and coexist.

Acknowledgments

This work is based on experiments performed at the Paul Scherrer Institut, Switzerland and has been supported by the Swiss National Foundation for Scientific Research within the NCCR MaNEP pool. The work at Stanford University was supported by the Department of Energy, Office of Basic Energy Sciences under contract DE-AC02-76SF00515.

References

[1] Norling B K and Steinfink H 1966 *Inorg. Chem.* **5** 1488
[2] DiMasi E, Aronson M C, Mansfield J F, Foran B and Lee S 1995 *Phys. Rev.* B **52** 14516
[3] Malliakas C, Billinge S J L, Kim H J and Kanatzidis M G 2005 *J. Am. Chem. Soc.* **127** 6510
[4] Ru N, Condron C L, Margulis G Y, Shin K Y, Laverock J, Dugdale S B, Toney M F and Fisher I R 2008 *Phys. Rev.* B **77** 035114
[5] Fang A, Ru N, Fisher I R and Kapitulnik A 2007 *Phys. Rev. Lett.* **99** 046401
[6] Ru N, Chu J H and Fisher I R 2008 *Phys. Rev.* B **78** 012410
[7] Banerjee A and Rosenbaum T, private communication
[8] Brouet V *et al* 2008 *Phys. Rev.* B **77** 235104
[9] Laverock J, Dugdale S B, Major Zs, Alam M A, Ru N, Fisher I R, Santi G and Bruno E 2005 *Phys. Rev.* B **71** 085114
[10] Johannes M D and Mazin I I 2008 *Phys. Rev.* B **77** 165135
[11] Ru N and Fisher I R 2006 *Phys. Rev.* B **73** 033101
[12] Iyeiri Y, Okumura T, Michioka C and Suzuki K 2003 *Phys. Rev.* B **67** 144417
[13] Deguchi K, Okada T, Chen G F, Ban D, Aso N and Sato N K 2009 *J. Phys. Conf. Ser.* **150** 042023
[14] Fischer P, Keller L, Schefer J and Kohlbrecher J 2000 *Neutron News* **11** 19
[15] Blau B *et al* 2009 *Neutron News* **20** 5
[16] Schefer J, Könnecke M, Murasik A, Czopnik A, Strässle Th, Keller P and Schlump N 2000 *Physica* B **276–278** 168
[17] Rodríguez-Carvajal J 1993 *Physica* B **192** 55
[18] Malliakas C and Kanatzidis M 2006 *J. Am. Chem. Soc.* **128** 12612
[19] Warren B E 1941 *Phys. Rev.* **59** 693
[20] Roessli B *et al* 1993 *Z. Phys.* B **91** 149
[21] Gignoux D and Schmitt D 1993 *Phys. Rev.* B **48** 12682
[22] Gignoux D and Schmitt D 1994 *J. Magn. Magn. Mater.* **129** 53